Hydrophilic bile acids prevent liver damage caused by lack of biliary phospholipid in $Mdr2^{-/-}$ mice[S]

Renxue Wang,* Jonathan A. Sheps,* Lin Liu,* Jun Han,[†] Patrick S. K. Chen,[§] Jason Lamontagne,[§] Peter D. Wilson,[§] Ian Welch,**,[††] Christoph H. Borchers,[†,§§,***] and Victor Ling[1,*,***]

BC Cancer Research Centre,* Vancouver, British Columbia, Canada; University of Victoria-Genome BC Proteomics Centre[†] and Department of Biochemistry and Microbiology,[§§] University of Victoria, Victoria, British Columbia, Canada; Department of Chemistry,[§] Simon Fraser University, Burnaby, British Columbia, Canada; Department of Pathology** and Centre for Comparative Medicine,[††] University of British Columbia, Vancouver, British Columbia, Canada; and Proteomics Centre, Segal Cancer Centre, Lady Davis Institute, Jewish General Hospital,*** McGill University, Montreal, Quebec, Canada

Abstract Bile acid imbalance causes progressive familial intrahepatic cholestasis type 2 (PFIC2) or type 3 (PFIC3), severe liver diseases associated with genetic defects in the biliary bile acid transporter bile salt export pump (BSEP; ABCB11) or phosphatidylcholine transporter multidrug resistance protein 3 (MDR3; ABCB4), respectively. $Mdr2^{-/-}$ mice (a PFIC3 model) develop progressive cholangitis, ductular proliferation, periportal fibrosis, and hepatocellular carcinoma (HCC) because the nonmicelle-bound bile acids in the bile of these mice are toxic. We asked whether the highly hydrophilic bile acids generated by $Bsep^{-/-}$ mice could protect $Mdr2^{-/-}$ mice from progressive liver damage. We generated double-KO (DKO: $Bsep^{-/-}$ and $Mdr2^{-/-}$) mice. Their bile acid composition resembles that of $Bsep^{-/-}$ mice, with increased hydrophilic muricholic acids, tetrahydroxylated bile acids (THBAs), and reduced hydrophobic cholic acid. These mice lack the liver pathology of their $Mdr2^{-/-}$ littermates. The livers of DKO mice have gene expression profiles very similar to $Bsep^{-/-}$ mice, with 4,410 of 6,134 gene expression changes associated with the $Mdr2^{-/-}$ mutation being suppressed. Feeding with THBAs partially alleviates liver damage in the $Mdr2^{-/-}$ mice.【JLR】 Hydrophilic changes to biliary bile acid composition, including introduction of THBA, can prevent the progressive liver pathology associated with the $Mdr2^{-/-}$ (PFIC3) mutation.—Wang, R., J. A. Sheps, L. Liu, J. Han, P. S. K. Chen, J. Lamontagne, P. D. Wilson, I. Welch, C. H. Borchers, and V. Ling. **Hydrophilic bile acids prevent liver damage caused by lack of biliary phospholipid in Mdr2−/− mice.** *J. Lipid Res.* 2019. 60: 85–97.

Supplementary key words   bile acids and salts/biosynthesis • cancer • gene expression • hepatic cellular carcinoma • hydrophobicity • inflammation • liver fibrosis • progressive familial intrahepatic cholestasis • tetrahydroxylated bile acids

Bile acids, the major organic solutes of bile, are amphipathic molecules derived from cholesterol. They function to drive bile flow, as detergents to aid digestion of fatty nutrients, and as signaling molecules to maintain lipid homeostasis (1, 2). Bile acids, especially the more hydrophobic ones, are lipolytic and are cytotoxic when in high concentrations. Thus, bile acids constitute a constant potential source of inflammatory stress in the liver, particularly in cholestatic conditions (1, 3, 4).

Progressive familial intrahepatic cholestasis (PFIC) is a group of heterogeneous genetic defects leading to imbalances in bile formation (5, 6). Three types of PFIC have been described: PFIC1, caused by mutations in the *ATP8B1* gene; PFIC2, caused by mutations in the *ABCB11* [bile salt export pump (*BSEP*)] gene; and PFIC3, caused by mutations in the *ABCB4* [multidrug resistance protein 3 (*MDR3*)] gene. Animal models, in which orthologs of these genes have been inactivated, have been generated. In the current study, we focus on the mouse models for PFIC2 and PFIC3.

The *ABCB11* gene, associated with PFIC2, encodes the major energy-dependent BSEP translocating bile salts across the canalicular membranes in the liver (7–9). This is the rate-limiting step in the enterohepatic circulation of bile salts and a major driving force for bile flow. Severe BSEP deficiency in humans causes a fatal childhood disease, PFIC2, with low or normal serum γ-glutamyl transferase (γ-GT), secretion of bile salts into the bile reduced to less than 1% of normal (10), hepatic inflammation, dilated canalicular lumens lacking microvilli (6, 11), and an increased propensity for developing hepatocellular carcinoma (HCC) (12) and cholangiocarcinoma (13). Unlike

Abbreviations: ALP, alkaline phosphatase; ALT, alanine aminotransferase; BSEP, bile salt export pump; CA, cholic acid; DKO, double KO; HCC, hepatocellular carcinoma; MCA, muricholic acid; MDR, multidrug resistance protein; PC, phosphatidylcholine; PFIC, progressive familial intrahepatic cholestasis; PSC, primary sclerosing cholangitis; RNA-Seq, RNA-sequencing; THBA, tetrahydroxylated bile acid; UDCA, ursodeoxycholic acid; UPLC/MRM-MS, ultra-high-performance liquid chromatography/multiple-reaction monitoring-mass spectrometry.

[1] To whom correspondence should be addressed.
    e-mail: vling@bccrc.ca
[S] The online version of this article (available at http://www.jlr.org) contains a supplement.

PFIC2 patients, mice with null mutations of the *Bsep* gene have normal life spans, generate adequate bile flow, do not exhibit progressive cholestasis, and do not develop HCC (9). These mice appear to shift the composition of their bile acids to a more hydrophilic (less toxic) one, notably by producing a novel class of tetrahydroxylated bile acids (THBAs), which, together with significant canalicular secretion of THBA via an alternative canalicular transporter mechanism, appears to protect the $Bsep^{-/-}$ mice from suffering the otherwise expected severe pathogenesis of PFIC2 (9, 14, 15).

The *ABCB4* gene associated with PFIC3 encodes MDR3, a protein functioning as a flippase translocating phosphatidylcholine (PC) into the bile (16). PC, together with cholesterol, is required to form mixed micelles with bile acids in the canaliculus to neutralize the toxic detergent effects of bile acids in the bile (3, 4). A lack of PC in the bile causes patients to develop a progressive disease that includes jaundice, pale stools, hepatosplenomegaly, pruritus, elevated serum bile acids, and elevated serum γ-GT. *ABCB4* deficiency can also result in formation of cholesterol gallstones, drug-induced cholestasis, and adult biliary cirrhosis (17). A genetic model for PFIC3 is the $Mdr2^{-/-}$ mouse, with an inactivated *Abcb4* gene, ortholog of the human *ABCB4*. These mice suffer from bile acid toxicity and develop liver lesions resembling those found in PFIC3 patients, featuring cholangitis, ductular proliferation and periportal fibrosis, formation of gallstones, and eventually HCC (16, 18, 19). As in PFIC3 patients, nonmicelle-bound cytotoxic bile acids in bile result in progressive liver injury. The $Mdr2^{-/-}$ mice develop severe periductular inflammation, starting from the second week of age (16, 20). Cholangiopathy progresses rapidly in the first several weeks of life. Because of the severe and progressive nature of the $Mdr2^{-/-}$ phenotype, these mice are often used as an efficacy model in the development of therapeutics for primary sclerosing cholangitis (PSC) (19, 21).

In this study, we asked whether the hepatoprotective bile acid composition of the $Bsep^{-/-}$ mice, involving high levels of hydrophilic bile acids such as THBAs, could prevent progression of cholangitis in the $Mdr2^{-/-}$ mice lacking PC. We therefore crossed a *Bsep* null mutation into the $Mdr2^{-/-}$ genetic background to create a double-KO (DKO; $Bsep^{-/-}$ and $Mdr2^{-/-}$) mouse. We followed the development of the homozygous DKO mice in comparison with their *Bsep* heterozygote or WT and $Mdr2^{-/-}$ littermates. The DKOs did not exhibit any features of the PSC-like progression seen in the $Mdr2^{-/-}$ mice, even after 13.5 months. We report here a detailed analysis of the histological, physiological, and genetic regulatory consequences of combining the $Bsep^{-/-}$ and $Mdr2^{-/-}$ mutant lines. Our observation is that, concomitant with a reduction of toxic bile acids in the bile canaliculi and cholangiocyte network, the $Bsep^{-/-}$ mutation suppresses almost all of the pathological signs associated with the $Mdr2^{-/-}$ phenotype at the histological, cellular, and genetic levels. We also fed $Mdr2^{-/-}$ mice with a novel synthetic THBA to examine whether addition of such a hydrophilic bile acid would also be able to alleviate cholangiocyte damage in the $Mdr2^{-/-}$ mice.

MATERIALS AND METHODS

Animal husbandry

Mice were maintained in a 12 h light and dark cycle, at 22°C, with access to food and water at liberty. The progression of liver damage seen in the $Mdr2^{-/-}$ mice is sensitive to sex (22), background genetics (19), and to the diet used (unpublished observation). For example, we noted that disease progression was slower when a relatively low-fat diet (LabDiet 5001, St. Louis, MO), such as is typically used for the maintenance of adult mice, was used, compared with the relatively high-fat Harlan diet (Teklad Global 2019 Extruded Rodent Diet, Harlan Laboratories, Teklad Diets, Madison, WI) routinely used for breeding pairs and adolescent mice in our facility. In this study, we only used female mice on the FVB genetic background maintained on the high-fat Harlan diet. Experiments were performed using approved protocols of the Committee on Animal Care, University of British Columbia, according to the guidelines of the Canadian Council on Animal Care.

Generation of DKO mice for the *Bsep* and *Mdr2* genes

DKO mice carrying null mutations of both the *Bsep* and *Mdr2* genes were generated by crossing $Bsep^{-/-}$ mice (9, 15) with $Mdr2^{-/-}$ mice (16, 22), both of which were congenic strains on an FVB/NJ genetic background. The null genotype of the DKO mice was confirmed by genomic PCR showing the absence of a WT allele for *Bsep* and *Mdr2* (supplemental Table S1) (9, 16).

We used female mice, which are the more severely affected sex on the FVB genetic background, for comparative analyses in the current study. The observations presented here also apply to male mice, but liver injury in male $Mdr2^{-/-}$ mice was generally milder (22). Our analyses focused on age groups of 8 weeks, 20 weeks, 40 weeks, and 13.5 months. We used littermates as controls. For simplicity of analysis, we combined the data obtained from 22 week old mice with those of 20 weeks; we also combined $Bsep^{+/-}$ with the WT ($Bsep^{+/+}$) littermates of $Bsep^{-/-}$ mice, as they were phenotypically indistinguishable (23), and for the same reason, we combined $Bsep^{+/-}/Mdr2^{-/-}$ with $Bsep^{+/+}/Mdr2^{-/-}$ littermates of the DKO ($Bsep^{-/-}/Mdr2^{-/-}$) mice.

Synthesis of 3α,6α,7α,12α-tetrahydroxy-5β-cholanoic acid and 3α,6β,7α,12α-tetrahydroxy-5β-cholanoic acid

The syntheses of 3α,6α,7α,12α-tetrahydroxy-5β-cholanoic acid and 3α,6β,7α,12α-tetrahydroxy-5β-cholanoic acid were based on those reported by Iida et al. and Aggarwal et al. (24, 25). This chemistry was performed on a subgram scale, and minor modifications were made to the reported experimental and purification procedures in order to optimize yields (Supplemental Material 2). The final compounds were purified by flash chromatography to achieve purity greater than 95% as indicated by ^{1}H NMR analysis and homogeneity by HPLC. Scale-up synthesis of 3α,6α,7α,12α-tetrahydroxy-5β-cholanoic acid for the feeding study was performed by UHN Shanghai R&D Co. Ltd., China.

Measurement of bile flow

Bile flow rates in WT mice, after 2–4 h of fasting, were measured using gall bladder cannulation as previously described (9). Briefly, the abdomen was opened, and the gall bladder was cannulated using a PE-10 catheter after distal common bile duct ligation (9). After 20 min of equilibration, bile was collected into pre-tared tubes at 5 min intervals for 10 min. A bolus of a bile acid, either ursodeoxycholic acid (UDCA) (Sigma-Aldrich, Darmstadt, Germany) or THBA, was injected into the tail vein over a 20 s interval. Bile was further collected through the cannula at 2 min intervals for 20 min, followed by 10 min intervals for 20 min.

THBA feeding

Female mice were fed a diet supplemented with 1% (wt/wt) 3α,6α,7α,12α-tetrahydroxy-5β-cholanoic acid (6α,7α-THBA), using the high-fat Harlan diet as the base diet, from week 3 to week 20, for 17 weeks.

Tissue collection, liver indicator tests, liver histology, and immunohistochemistry

After 2–4 h fasting, fresh fecal samples were collected, weighed, and snap-frozen in liquid nitrogen, and stored at −80°C until further analysis. Mice were euthanized with an overdose of anesthetic. Blood was collected by cardiac puncture, and plasma was obtained by centrifugation at 12,000 g for 5 min, using a benchtop centrifuge.

After bleeding, the liver was carefully removed and weighed, the gall bladder was separated, and bile was collected. Two slices of the left lateral lobe were fixed in 10% neutral buffered formalin for 40–48 h and then transferred to 70% ethanol for paraffin embedding and staining with H&E and Sirius Red. Remaining left lateral lobe and other lobes were snap frozen in liquid nitrogen and stored at –80°C. Liver indicator tests were performed by IDEXX Laboratories Canada (Markham, Ontario, Canada). Histopathological assessment was conducted independently by a certified pathologist (I.W.) and scored for five histopathological parameters using the scoring system reported by van Nieuwerk et al. (22).

For immunostaining, 5 μm tissue sections were stained with polyclonal rabbit anti-cytokeratin antibody (Dako) in a dilution of 1:400, followed by biotinylated anti-rabbit IgG in a dilution of 1:200 (Vector). Binding of the pan-CK antibody was detected by using the ABC kit (Vector, CA) with DAB (DAKO) as a substrate (Sigma, Canada).

Bile acid analysis

Bile acid analysis in the plasma, liver, bile, and feces were performed by ultra-high-performance liquid chromatography/multiple-reaction monitoring-mass spectrometry (UPLC/MRM-MS) using the procedure previously reported (26). The quantitation of bile acids utilized 60 bile acid standards and 14 deuterium-labeled analogs as internal standards. The 60 targets included all of the major bile acids and some atypical ones, such as THBAs (26, 27).

RNA analysis

RNA-sequencing (RNA-Seq) analysis was undertaken in order to interrogate the total complement of genes expressed in a quantitative and unbiased manner (28). This allows for the discovery of gene expression changes not previously reported or anticipated. Total RNA was isolated as previously described using a Qiagen RNeasy Mini Kit (Toronto, Ontario, Canada) (15). Gene expression analysis by RNA-Seq was performed by Novogene (Sacramento, CA), using their standard protocol (Supplemental Material 1). Paired-end reads (75 bp from each end) were obtained from cloned fragments on an Illumina HiSeqTM2500 machine, and raw reads were stored as FASTQ files. P values were adjusted for multiple testing in order to control the false discovery rate (29, 30). Only genes with adjusted P values <0.05 were considered.

Statistical analysis

Data, other than RNA-Seq, are presented as means ± SD of the mean. One-way ANOVA tests were used for multiple comparisons. Student's t or Fisher's exact test was used for comparison between the DKO mice and their $Mdr2^{-/-}$ littermate controls.

RESULTS

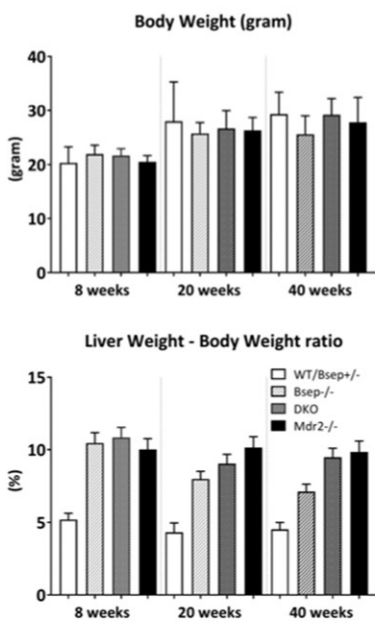### Progression of liver injury in Mdr2$^{-/-}$ mice

The $Mdr2^{-/-}$ mice exhibit characteristic stage-specific liver injuries (18) (**Fig. 1**), although the progression of disease can differ significantly, depending on sex, genetic background, and diet (see Materials and Methods). Under the conditions used in the current study, $Mdr2^{-/-}$ FVB mice develop inflammation in the portal triads, ductular proliferation, and periportal fibrosis as early as 3 weeks, with fibrosis progressing rapidly in the first several weeks, up to 10–12 weeks, and peaking around 20 weeks (Fig. 2D). The progression of liver injury in our mice appears to be more rapid than reported previously (22), which may be due to our maintaining the mice on the high-fat Harlan diet (see Materials and Methods). Our $Mdr2^{-/-}$ mice all displayed advanced inflammation in portal triads and periportal fibrosis at 8 weeks of age, and 40% developed gallstones (Table 1). The faster progression observed in our mice was reflected also in their liver indicator profiles. For instance, the average alkaline phosphatase (ALP) and alanine aminotransferase (ALT) were both ∼400 IU/l (Fig. 1B) in the plasma, twice as high as those of the same sex reported by van Nieuwerk et al. (22).

Bsep inactivation reversed bile acid toxicity caused by *Mdr2* null mutation in DKO mice
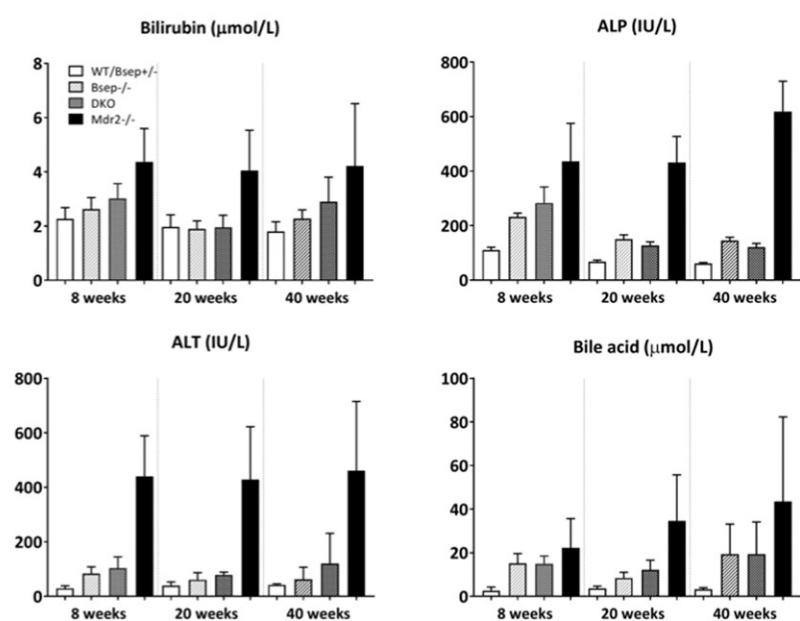
DKO mice exhibited liver enlargement, similar to $Mdr2^{-/-}$ controls and $Bsep^{-/-}$ mice, and at 8 weeks their relative liver weight (liver to body weight ratio) was around 10% (Fig. 1A), whereas the relative liver weight of WT mice was typically around 5%. As the animals grew, the relative liver weight of $Bsep^{-/-}$ mice improved to about 7%, at 40 weeks, significantly better than the $Mdr2^{-/-}$ and DKO mice which remained at about 10% (Fig. 1A). Although their livers were enlarged, the DKO mice suffered minimal liver damage with near normal liver indicator profiles in the plasma, generally much lower than their $Mdr2^{-/-}$ littermates and closer to WT levels (Fig. 1B). Specifically, DKO mice had significantly lower ALP and ALT than their $Mdr2^{-/-}$ littermates. Liver indicators in the DKO mice did not increase with age, suggesting a lack of progressive liver damage. The lack of progression in DKO mice is also supported by histological evidence (**Fig. 2** and supplemental Fig. S1C–G). Immunostaining indicated that the $Bsep^{-/-}$ genotype prevented ductular proliferation in the DKO mice (Fig. 2E, F).

Even at the age of 13.5 months, the livers and gall bladders of DKO mice appeared to be relatively normal, in sharp contrast to their $Mdr2^{-/-}$ littermates, where livers with multiple large nodules and gall bladders with discolored bile were observed (supplemental Fig. S1A, B). The DKO mice did not develop liver nodules or neoplastic lesions in any age group examined, whereas in the $Mdr2^{-/-}$ controls, 50% of the mice developed multiple neoplastic lesions and nodules at 40 weeks (**Table 1**). At the age of 13.5 months, 100% of $Mdr2^{-/-}$ mice carried multiple liver tumor nodules, with the largest observed often 1–2 cm in diameter (Table 1; supplemental Fig. S1). Histologically,

A   Body weight, and relative liver weight

Body Weight (gram)

Liver Weight - Body Weight ratio

B   Liver indicators of DKO mice

Bilirubin (μmol/L)

ALP (IU/L)

ALT (IU/L)

Bile acid (μmol/L)

Legend: □ WT/Bsep+/-; ▨ Bsep-/-; ▨ DKO; ■ Mdr2-/-

P values using one-way ANOVA multiple comparisons:

Age		A. Liver weight/body weight ratio				B.	Bilirubin			ALT			ALP			Bile acids		
		(n)	WT	Bsep⁻ᐟ⁻	DKO	(n)	WT	Bsep⁻ᐟ⁻	DKO	WT	Bsep⁻ᐟ⁻	DKO	WT	Bsep⁻ᐟ⁻	DKO	WT	Bsep⁻ᐟ⁻	DKO
8 wks	(n)	(n=10)	(n=5)	(n=6)		(n=9)	(n=9)	(n=4)	(n=6)	(n=9)	(n=4)	(n=6)	(n=9)	(n=4)	(n=6)	(n=9)	(n=4)	(n=6)
	Bsep⁻ᐟ⁻	(n=5)	****	-		(n=4)	ns	-		ns	-		ns	-		ns	-	
	DKO	(n=6)	****	ns	-	(n=6)	ns	ns	-	ns	ns	-	****	**	-	*	ns	-
	Mdr2⁻ᐟ⁻	(n=11)	****	ns	ns	(n=7)	****	**	*	****	****	****	****	**	*	***	ns	ns
20 wks	(n)	(n=9)	(n=7)	(n=8)		(n=4)	(n=4)	(n=4)	(n=7)	(n=4)	(n=4)	(n=7)	(n=4)	(n=4)	(n=7)	(n=4)	(n=4)	(n=7)
	Bsep⁻ᐟ⁻	(n=7)	****	-		(n=4)	ns	-		ns	-		ns	-		ns	-	
	DKO	(n=8)	****	*	-	(n=7)	ns	ns	-	ns	ns	-	ns	ns	-	ns	ns	-
	Mdr2⁻ᐟ⁻	(n=27)	****	****	**	(n=13)	ns	ns	**	***	***	****	****	****	****	**	*	*
40 wks	(n)	(n=8)	(n=4)	(n=5)		(n=3)	(n=3)	(n=4)	(n=4)	(n=3)	(n=4)	(n=4)	(n=3)	(n=4)	(n=4)	(n=3)	(n=4)	(n=4)
	Bsep⁻ᐟ⁻	(n=4)	****	-		(n=4)	ns	-		ns	-		ns	-		ns	-	
	DKO	(n=5)	****	****	-	(n=4)	ns	ns	-	ns	ns	-	ns	ns	-	ns	ns	-
	Mdr2⁻ᐟ⁻	(n=9)	****	****	ns	(n=5)	ns	ns	ns	*	*	*	****	****	****	ns	ns	ns

Fig. 1. Body weights, relative liver weights (liver to body weight ratios, percent), and liver indicators of DKO ($Bsep^{-/-}$ and $Mdr2^{-/-}$) mice and their parental genotypes. A: Body weights and relative liver weight of DKO mice at the ages of 8, 20, and 40 weeks, in comparison with control $Mdr2^{-/-}$, $Bsep^{-/-}$, and WT mice. B: Liver indicators of DKO mice in comparison with parental genotypes at 8, 20, and 40 weeks of age. Bilirubin, ALP, ALT, and total plasma bile acids are measured. Table indicates statistical significance between genotypes obtained by one-way ANOVA tests. * $P < 0.05$; ** $P < 0.01$; *** $P < 0.001$; **** $P < 0.0001$. ns, not significant.

DKO mice, at any age up to 13.5 months, did not display any of the liver damage commonly seen in $Mdr2^{-/-}$ mice (supplemental Fig. S1). In addition, we very rarely observed gallstone formation in DKO mice, across all age groups examined (only one case observed), whereas in the $Mdr2^{-/-}$ controls, the gallstone rate increased from 40% at the age of 8 weeks to 100% at 40 weeks (Table 1).

Hydrophilic shift in the bile acid composition of DKO mice

The DKO mice suffered no significant liver injury, despite carrying the $Mdr2^{-/-}$ mutation and a lack of PC in the bile to neutralize the toxicity of their bile acids. To gain an insight into how such hepatic protection is achieved, we measured the bile acid composition in the DKO mice using UPLC/MRM-MS (26). We found that total bile acid concentrations in the liver and plasma of DKO, $Bsep^{-/-}$, and

$Mdr2^{-/-}$ mice at 8 weeks of age were significantly higher, compared with the WT, indicating that these KO mice all suffered from some degree of cholestasis (**Fig. 3A**). For example, bile acid concentrations in $Mdr2^{-/-}$ mice were 19-fold higher in the plasma and 5-fold higher in the liver, compared with WT. Accumulation of total bile acids in the liver of the DKO mice, like in the $Bsep^{-/-}$ mice, was 3-fold higher still than that of the $Mdr2^{-/-}$ mice, which is consistent with a lower fecal bile acid level in the DKO and $Bsep^{-/-}$ mice (Fig. 3A). However, the DKO mice suffered none of the histological liver damage observed in the $Mdr2^{-/-}$ mice (Fig. 2).

It appears that the 3-fold increase of bile acids in the liver of DKO mice was due primarily to increased production of hydrophilic bile acids, THBAs, and β-muricholic acid (β-MCA) (Fig. 3B), with about a 50% decrease in the production of hydrophobic cholic acid (CA). This hydrophilic
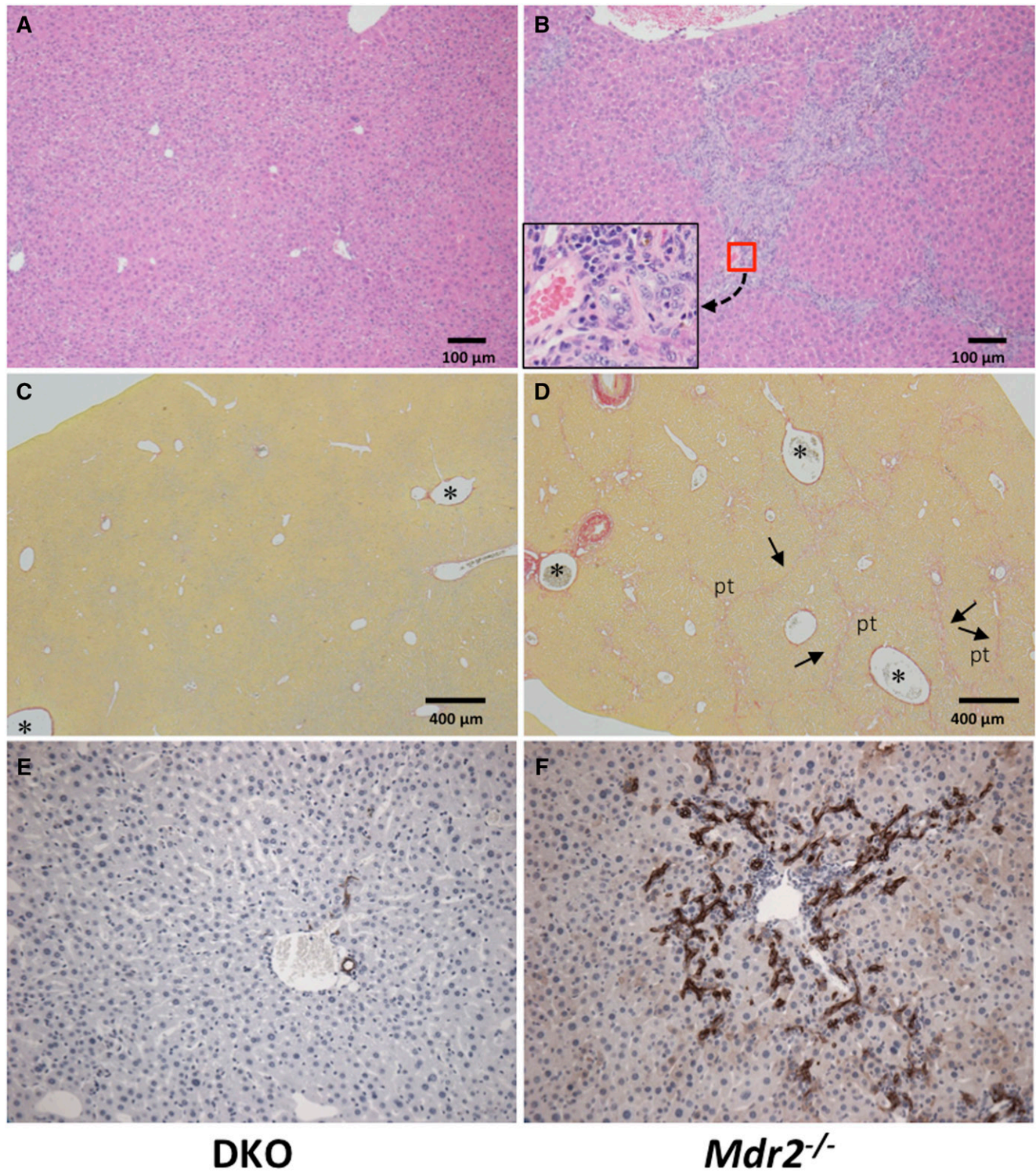
Fig. 2. Histology and immunohistochemistry of the livers of the DKO mice (A, C, E) compared with the livers of $Mdr2^{-/-}$ mice (B, D, F) at the age of 20 weeks. H&E staining: DKO mouse showing normal liver morphology (A) and $Mdr2^{-/-}$ liver with an inset showing marked inflammatory cell infiltration (B). C: Sirius Red-stained DKO liver with no detectable fibrosis. D: Sirius Red-stained $Mdr2^{-/-}$ liver displayed stage 3 bridging fibrosis, according to the scale of van Nieuwerk et al. (22). Arrows, bridging fibrosis; pt, portal triads; asterisks, central vein. E, F: Anti-pan-CK immunostaining (dark brown staining) showing normal morphology in the DKO liver and extensive ductular proliferation in the $Mdr2^{-/-}$ liver (20×), respectively.

shift in the bile acid composition in the livers of DKO mice resulted in a bile that is essentially nontoxic, even though the level of bile acids in the liver of these mice was about 15-fold higher than WT. The bile acid composition of the $Mdr2^{-/-}$ mice, on the other hand, remained similar to WT, with relatively high levels of hydrophobic CA and about the same proportion of β-MCA (Fig. 3B). Similarly the CA levels in the bile of $Bsep^{-/-}$ and DKO mice were very much

TABLE 1. Rates of gallstone and nodule formation in DKO mice

Age	Gallstones			Nodules		
	DKO	Control $Mdr2^{-/-}$	$P*$	DKO	Control $Mdr2^{-/-}$	$P*$
8 weeks	0% (0/4)	40% (4/10)	>0.25	0% (0/4)	0% (0/10)	>0.9999
20 weeks	14.3% (1/7)	81.5% (22/27)	0.002	0% (0/7)	3.7% (1/27)	>0.9999
40 weeks	0% (0/5)	100% (10/10)	0.0003	0% (0/5)	50% (5/10)	0.1009
13.5 months	0% (0/4)	88.9% (8/9)	0.007	0% (0/4)	100% (11/11)	0.0007

*P values were obtained using Fisher's exact test.

lower than in $Mdr2^{-/-}$ and WT mice, whereas the THBA levels were much higher (Fig. 3B). Thus, it appears that the hydrophilic shift in bile acid composition in DKO mice protects them from developing the PSC-like progression seen in $Mdr2^{-/-}$ mice.

Comparative gene expression profiling by RNA-Seq analysis

In order to characterize the $Bsep^{-/-}$ and $Mdr2^{-/-}$ mice in greater detail, we undertook comprehensive RNA-Seq analyses of expressed genes in the livers of all four groups of mice. Cluster analysis shows that the Pearson correlation ($R^2 = 0.983$ or greater) between individual mouse samples, by gene expression, demonstrated the coherence of each group, and thus the recessivity of both $Mdr2^{-/-}$ and $Bsep^{-/-}$ mutations (supplemental Fig. S2). RNA-Seq results of individuals from each group were pooled for analysis.

The overall finding is that the principal consequence of introducing the $Bsep^{-/-}$ mutation onto the $Mdr2^{-/-}$ background is to suppress over 4,000 changes in gene expression associated with the $Mdr2^{-/-}$ mutation. $Bsep^{-/-}$ mice exhibit significant expression changes in 2,545 genes, relative to their phenotypically WT littermates. $Mdr2^{-/-}$ mutation, however, results in differential expression of 6,134 genes. Remarkably, comparing $Bsep^{-/-}$ mice with DKO mice found only 141 differentially expressed genes (see volcano plots in supplemental Fig. S3 A–D). Thus, the $Bsep$ mutation acts epistatically to suppress much of the $Mdr2^{-/-}$ phenotype. Of the 6,134 gene expression changes associated with $Mdr2$ mutation, 1,659 were common changes also observed in $Bsep^{-/-}$ mice, and of the other 4,475 changes that differentiate the $Mdr2^{-/-}$ mouse from both WT and $Bsep^{-/-}$ mice, only 65 remained significantly altered in the DKO (supplemental Fig. S3E and Table S5). The differential expression of these 65 genes presumably reflects the underlying defect in MDR2 transporter function, independent of the liver pathology caused by toxic bile acids.

The compensating regulatory responses that protect the $Bsep^{-/-}$ mouse from developing a PFIC2-like liver pathology may be deduced from the gene expression data, and these were generally shared with the DKO mice (supplemental Table S4 and **Fig. 4**). Changes in expression of over 170 genes, ordered into 11 functional categories relevant to liver function in $Mdr2^{-/-}$ mice, are shown in supplemental Table S4. These include categories such as cytochrome P450 enzymes, cholesterol and lipoprotein metabolism, nuclear receptors, hepatocyte-expressed transporters, inflammatory response genes, fibrosis-related genes, etc. (supplemental Table S4). The variation in expression of

this set of genes across all 16 mice used in our study is further illustrated in the form of a heatmap (Fig. 4). The genes in this figure are not necessarily the most representative of the overall pattern of expression changes seen in this dataset, but the broad tendency for expression in the DKO liver to resemble that of the $Bsep^{-/-}$, more than the $Mdr2^{-/-}$, mouse liver is still evident.

Specifically, there is an upregulated gene expression of cytochrome P450 oxidases involved in the hydroxylation of bile acids, particularly the $Cyp2c$ family ($Cyp2c29$, $Cyp2c37$, $Cyp2c38$, $Cyp2c40$, $Cyp2c50$, $Cyp2c54$, $Cyp2c55$, $Cyp2c68$, and $Cyp2c69$) (31) and $Cyp3a11$ (32); ABC transporters involved in the apical ($Mdr1a$) and basolateral ($Mrp3$, $Mrp4$ and $Ost\beta$) export of bile acids (33–35); as well as phase II detoxification enzymes responsible for sulfation ($Sult2a1$ and $Sult2a2$) (36), glucuronidation ($Ugt1a1$ and $Ugt1a5$) (37) and glutathione conjugation, of bile acids ($Gsta1$, $Gsta2$, and $Gstm3$) (38, 39).

Both MDR1 and MRP2 have been proposed as possible apical exporters for the THBA that dominates the bile acid pool in $Bsep^{-/-}$ mice (9, 14, 40). In the $Bsep^{-/-}$ and DKO mice, we find that $Mdr1a$ is upregulated, to a greater extent than in $Mdr2^{-/-}$ mice, whereas $Mdr1b$ is upregulated in DKO and $Mdr2^{-/-}$ mice, but essentially unchanged in $Bsep^{-/-}$ mice. $Mrp2$ remained unchanged in all three mutant strains.

Higher production of biliary CA, relative to β-MCAs and/or THBAs, in the $Mdr2^{-/-}$ mice relative to the DKO, was reflected in the underlying genetic regulatory responses of these two genotypes. In all three KO mouse strains examined, the bile acid synthetic enzyme $Cyp7a1$ (41) was upregulated, which seems paradoxical as a response to cholestasis; however, this was compensated for by downregulation of downstream enzymes, particularly Cyp8b1, responsible for CA synthesis, which was particularly marked in the $Bsep^{-/-}$ strain. $Cyp7b1$ and $Cyp27a1$, enzymes of the muricholic acid (MCA) synthesis pathways (41), were also downregulated in all three strains, but more so in the $Mdr2^{-/-}$ mouse, indicating a shift toward CA synthesis over β-MCA, relative to WT, and a shift in the opposite direction, toward β-MCA in the $Bsep^{-/-}$ strain and, to a lesser extent, in the DKO. The DKO mouse had a higher β-MCA:CA ratio in its bile (Fig. 3B). It is notable that $Cftr$ expression, which is involved in a CA-induced increase in biliary secretion, and liver growth response, in mice (42) rose to 14 times normal in the $Mdr2^{-/-}$ mice, three times above normal in the DKO mice and fell to 0.6× of normal in $Bsep^{-/-}$ mice (supplemental Table S4).

In addition, a subset of differentially expressed genes, known to be of some significance for the development of
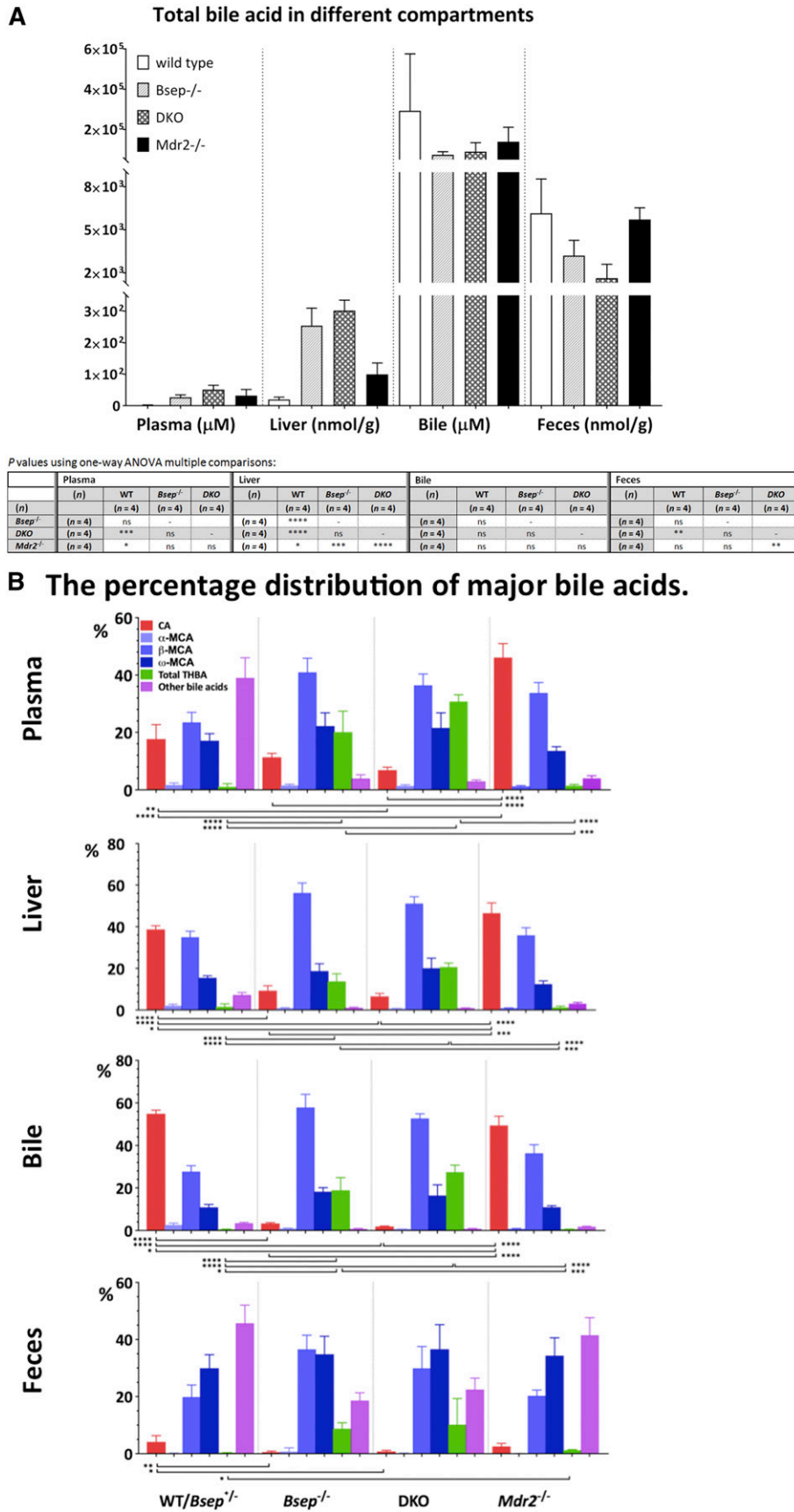
A Total bile acid in different compartments

Legend: □ wild type; (hatched) Bsep-/-; (crosshatch) DKO; ■ Mdr2-/-

P values using one-way ANOVA multiple comparisons:

	Plasma				Liver				Bile				Feces			
(n)	(n)	WT	Bsep-/-	DKO	(n)	WT	Bsep-/-	DKO	(n)	WT	Bsep-/-	DKO	(n)	WT	Bsep-/-	DKO
		(n = 4)	(n = 4)	(n = 4)		(n = 4)	(n = 4)	(n = 4)		(n = 4)	(n = 4)	(n = 4)		(n = 4)	(n = 4)	(n = 4)
Bsep-/-	(n = 4)	ns	-		(n = 4)	****	-		(n = 4)	ns	-		(n = 4)	ns	-	
DKO	(n = 4)	***	ns	-	(n = 4)	****	ns	-	(n = 4)	ns	ns	-	(n = 4)	**	ns	-
Mdr2-/-	(n = 4)	*	ns	ns	(n = 4)	*	***	****	(n = 4)	ns	ns	ns	(n = 4)	ns	ns	**

B The percentage distribution of major bile acids.

Legend: CA; α-MCA; β-MCA; ω-MCA; Total THBA; Other bile acids

Plasma / Liver / Bile / Feces

WT/Bsep+/-   Bsep-/-   DKO   Mdr2-/-

Fig. 3. Bile acid profiles in different compartments of the DKO and their $Mdr2^{-/-}$ controls, $Bsep^{-/-}$, and their controls ($n = 4$ per genotype), measured using UPLC/MRM-MS. A: Total bile acids in the plasma, liver, bile, and feces of female mice at 8 weeks of age. B: The percentage distribution of major bile acids. Asterisks indicate the statistical significance between genotypes obtained by one-way ANOVA tests. * $P < 0.05$; ** $P < 0.01$; *** $P < 0.001$; **** $P < 0.0001$. ns, not significant.
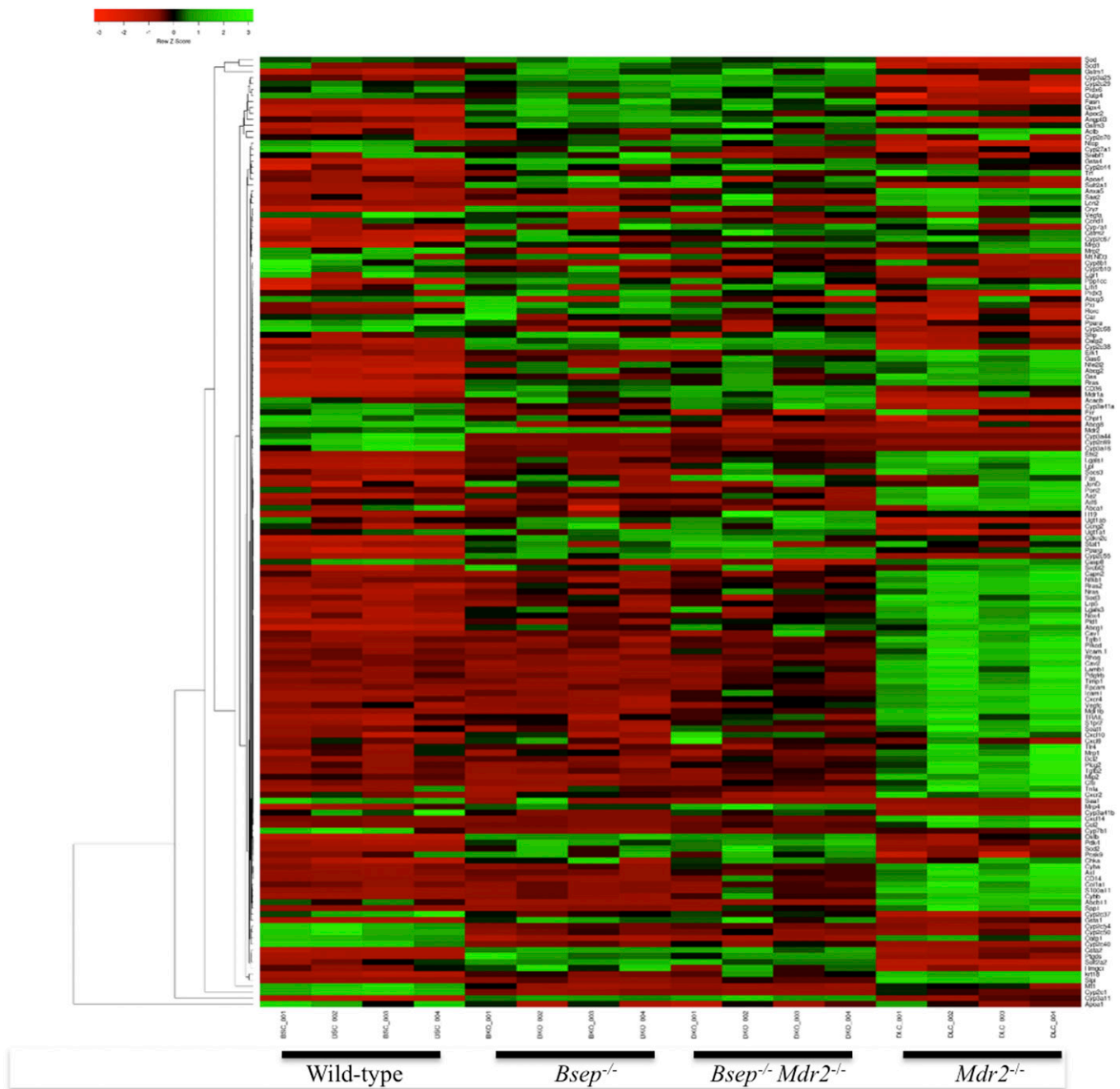
Fig. 4. Heatmap of expression changes among genes associated with liver phenotypes. Genes displayed are those listed in supplemental Table S3. Columns represent individual liver samples from 8-week-old female mice, four of each genotype. Genes are clustered according to their expression patterns, determined by RNA-Seq analysis, using the web service Heatmapper (http://www.heatmapper.ca/expression/) (54) with the default settings (Euclidean distances and average linkage).

liver pathology in the $Mdr2^{-/-}$ mice, finds several instances of the general where the DKO mouse tends to either return toward the WT or to adopt the $Bsep^{-/-}$ pattern of gene expression. These include genes involved in cholesterol synthesis (*Hmgcr*), FA metabolism (*Pxr*), basolateral import of bile acids (*Ntcp. Oatp1, Oatp2,* and *Oatp4*), markers of inflammation (*Ccl2, Nfκb1, Pdgfβ, Spp1, Tlr4, Tnfα, Vegfc, Cxcr2, Cxcr4, Cxcl2, Cxcl4, Icam1, Cd14,* and several others), proliferation (*Ccnd1, Egr1, Ets2,* and *S100a11*), fibrosis (*Tgfβ1, Tgfβ2, Col1a1* and *Timp*), and apoptosis (*Krt18* and *Trail*) (Fig. 4 and supplemental Table S4).
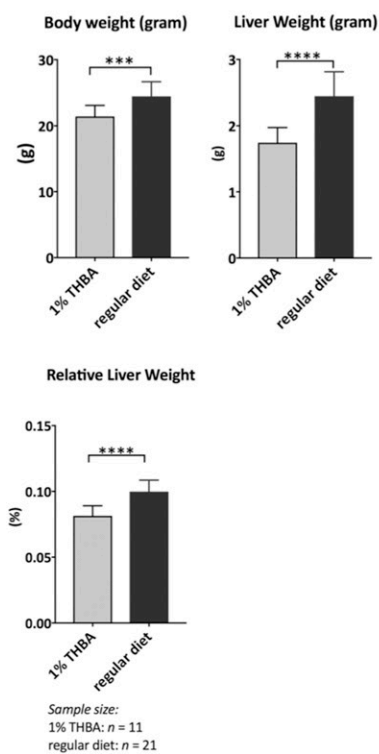
THBAs are hydrophilic choleretic agents

The $Bsep^{-/-}$ mice produce a large amount of THBA, which is associated with a much less severe cholestatic outcome compared with the consequences of null mutations in human *BSEP* (9, 14, 15, 43). To demonstrate the properties of THBA and to evaluate their potential therapeutic benefits, we synthesized two stereoisomers of THBA (see Materials and Methods). We examined whether or not administered THBA can promote bile flow, as other bile acids do, in WT FVB mice. As shown in **Fig. 5A**, the iv injection of either THBA compound resulted in an immediate and marked
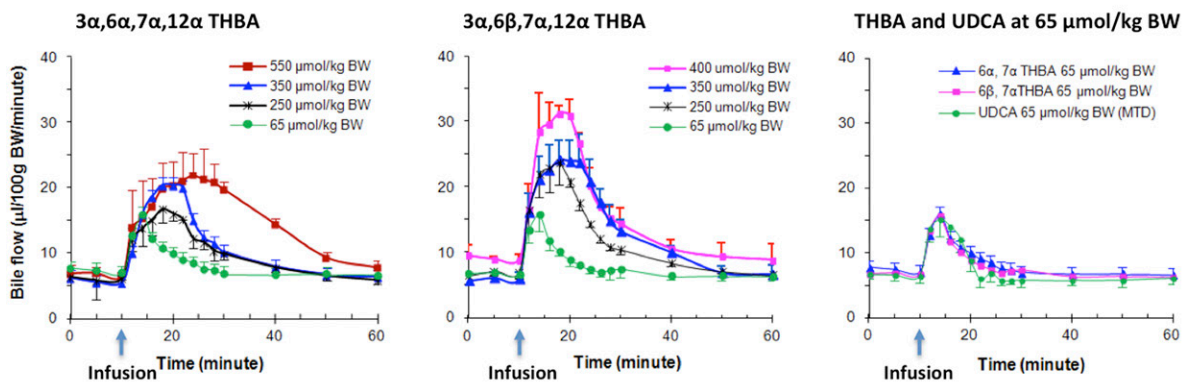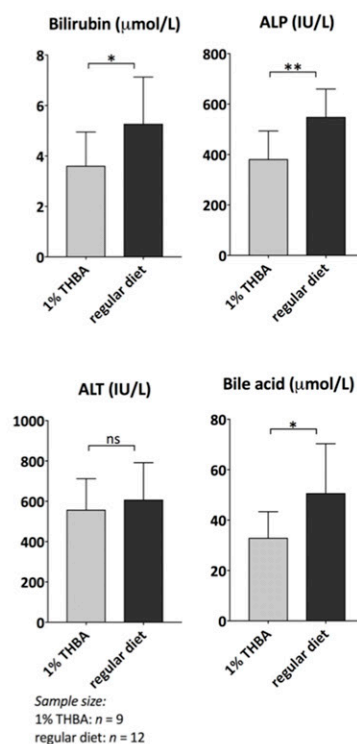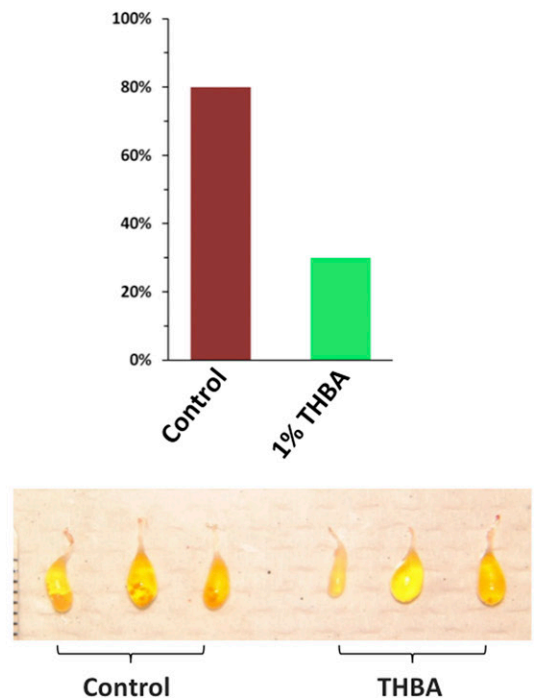
Fig. 5. Choleretic activity of THBA and characterization of $Mdr2^{-/-}$ mice fed either a 1% THBA diet or control diet. A: Synthetic $3\alpha,6\alpha,7\alpha,12\alpha$-THBA and $3\alpha,6\beta,7\alpha,12\alpha$-THBA can stimulate bile flow in a dose-dependent fashion in WT mice. They displayed a very similar potency to UDCA in stimulating bile flow after iv injection of 65 μmol/kg body weight, the maximum nonlethal dose of UDCA in this assay. B: Body weight, liver weight, and relative liver weight (liver to body weight ratios, percent). C: Liver indicators in the plasma of $Mdr2^{-/-}$ mice fed a 1% THBA diet or the control diet. D: Feeding of 1% THBA reduced gallstone formation and resulted in healthier gallbladders, with clearer bile, in the $Mdr2^{-/-}$ mice. Asterisks indicate the statistical significance between THBA-fed and regular diet-fed groups obtained by Student t-tests. * $P < 0.05$; ** $P < 0.01$; *** $P < 0.001$; **** $P < 0.0001$. ns, not significant.

increase in bile flow in WT mice in a dose-dependent fashion. The degree of bile flow stimulation by THBA was, on an equimolar basis, equivalent to that of UDCA. Interestingly, the dose dependencies of the two tested THBAs behaved differently: $6\alpha,7\alpha$-THBA had a greater effect on the time interval of bile flow, but $6\beta,7\alpha$-THBA affected the maximum flow rate (Fig. 5A). HPLC analysis of bile collected after iv injection of THBA showed that recovered THBA was predominantly in the taurine-conjugated form (data not shown).

These results are consistent with the idea that injected THBAs in mice are metabolized similarly to other bile acids, including their rapid uptake into the liver, subsequent taurine conjugation, and transport into the bile canaliculus, principally by a functional Bsep in the WT mice, to drive bile flow.

THBA feeding reduced liver damage in the $Mdr2^{-/-}$ mice

To determine whether or not the high levels of THBA found in DKO mice played a functional role in alleviating

liver damage caused by *Mdr2* mutation, we supplemented the diet of female *Mdr2*$^{-/-}$ mice with synthetic 6α,7α-THBA (1% by weight). The mice were fed for 17 weeks starting at 3 weeks of age, when the mice had already developed cholangiocyte damage (16, 20). Feeding *Mdr2*$^{-/-}$ mice with THBA resulted in significantly reduced body weights, liver weights, and relative liver weights. The relative liver weights were 8.1%, on average, compared with 10% of the *Mdr2*$^{-/-}$ mice fed the control diet (Fig. 5B). This reduced relative liver weight was associated with an improved liver indicator profile in the plasma of THBA-fed *Mdr2*$^{-/-}$ mice, notably, reduced ALP, consistent with reduced cholangiocyte damage, reduced bilirubin, and, interestingly, reduced total bile acids in plasma, despite high-dose feeding of a bile acid, i.e., THBA (Fig. 5C). Significantly less gallstone formation (30% vs. 80%) (Fig. 5D), compared with *Mdr2*$^{-/-}$ mice on the control diet, was also noted in the THBA-fed mice. However, no significant difference in the extent of liver fibrosis was observed between THBA-fed and control mice, using a semiquantitative scoring system (the scoring system used in supplemental Table S3) (22).

We further analyzed the bile acid profiles of the *Mdr2*$^{-/-}$ mice fed THBA using UPLC/MRM-MS. It was found that the THBA-fed *Mdr2*$^{-/-}$ mice had significantly reduced total bile acid in plasma, consistent with a relief in cholestasis. There were no significant changes in the concentration of bile acids in the liver and bile (**Fig. 6A**). However, significant changes to the bile acid composition can be seen in these latter two compartments (Fig. 6B). In the liver, the THBA level increased, whereas in the bile, the CA level decreased in both instances, leading to a more hydrophilic bile acid composition. The underlying causes of these changes are currently not understood, but, collectively, these changes appear to result in an overall reduced hydrophobicity and, presumably, less toxicity, of bile acids, particularly in the bile, of *Mdr2*$^{-/-}$ mice fed with THBA. Unsurprisingly, THBA-fed mice had greatly increased levels (about 45×) of bile acid in feces, which appears to be almost entirely made up of THBA (Fig. 6B).

DISCUSSION

Genetic defects in the canalicular transporters BSEP (ABCB11) and MDR3 (ABCB4) can cause fatal childhood diseases—PFIC2 or PFIC3, respectively. Mouse models of human genetic defects often do not mimic the behavior of their human counterparts. The inactivation of the mouse ortholog of *ABCB11* (*Bsep*$^{-/-}$), the major bile transporter, results in greatly impaired biliary secretion of bile acids, but with only mild cholestasis and no evident liver injury. Null mutation of *ABCB4* (*Mdr2*$^{-/-}$), on the other hand, results in compromised biliary secretion of PC to form mixed micelles with bile acids in bile, the absence of which subsequently causes severe and progressive bile duct damage due to the inherent detergent-like toxicity of unmasked bile acids. The phenotype of *Mdr2*$^{-/-}$ mice resembles chronic PSC (16, 18, 19), eventually leading to HCC (16,
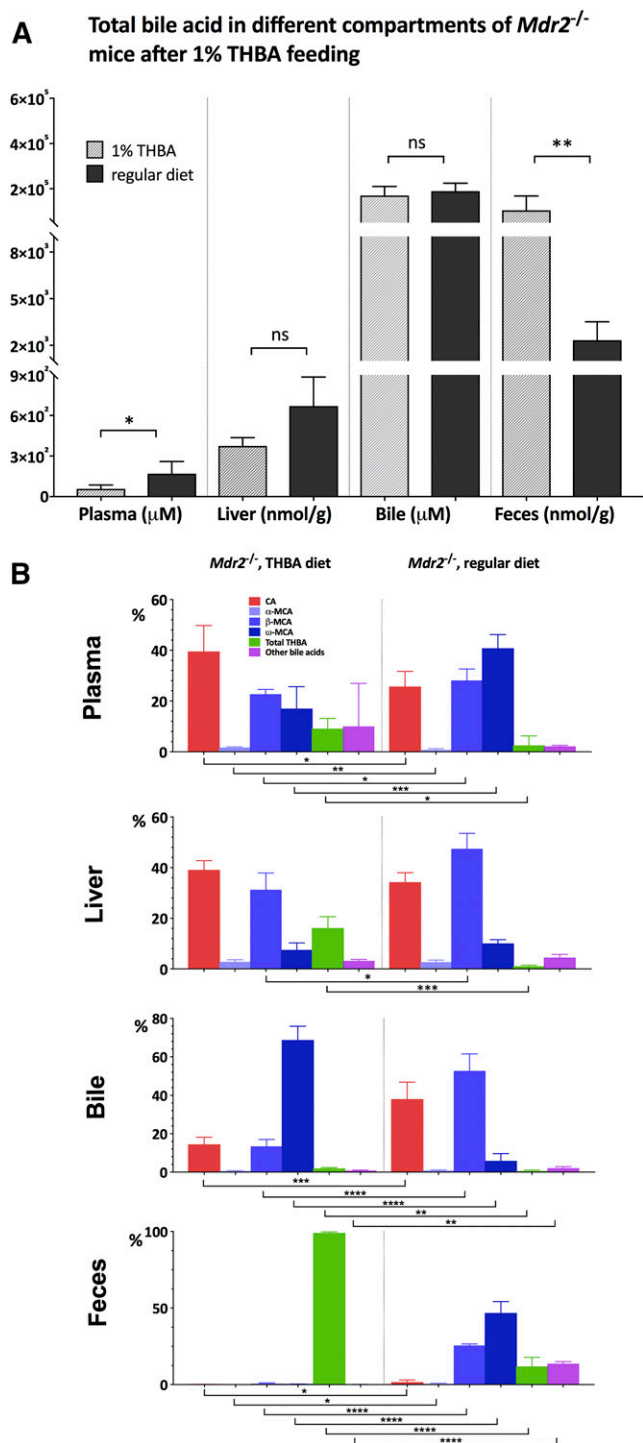

Fig. 6. A: Total bile acids in the plasma, bile, and feces of female *Mdr2*$^{-/-}$ mice, at 20 weeks of age, after 17 weeks fed a 1% THBA supplemented diet, or the control diet, measured using UPLC/MRM-MS (*n* = 5 per group). B: Percentage distribution of major bile acids. Asterisks indicate the statistical significance between THBA-fed and regular diet-fed groups obtained by Student *t*-tests. * *P* < 0.05; ** *P* < 0.01; *** *P* < 0.001; **** *P* < 0.0001. ns, not significant.

18, 19, 44). Over 6,100 gene expression changes are observed in the hepatocytes of these mice at 8 weeks, compared with WT (supplemental Fig. S3B), in response to the toxic effects of unmasked bile acids.

On the other hand, the mouse model of PFIC2, the $Bsep^{-/-}$ mouse, displays only a mild phenotype, with no progressive liver damage. A key feature of the hepatoprotective mechanism in the $Bsep^{-/-}$ mice appears to be the ability of their hepatocytes to shift the composition of their bile acid to a more hydrophilic, and less toxic, one by up-regulating a series of P450 enzymes, favoring production of the less hydrophobic primary bile acids (β-MCA over CA) and conversion of trihydroxy bile acids into THBAs (45). The reduced hepatoxicity of these bile acids is significant because these mice do have 5-fold higher levels of bile acids in the liver, but they do not suffer the pathology expected of a cholestatic phenotype. Moreover, the coordinated response of an upregulated Mdr1, the presumptive canalicular alternative transporter, working in concert with this change in bile acid composition, enables moderate biliary secretion of hydrophilic bile acids, reduces cholestasis, and prevents liver injury when the normal bile acid transporter Bsep is impaired (1, 9, 43).

In the present study, we asked whether the hydrophilic bile acids of the $Bsep^{-/-}$ mice could protect the liver of $Mdr2^{-/-}$ mice from suffering a PSC-like progression, in an environment where micelle-forming PC in the bile does not attenuate the detergent-like properties of these hydrophilic bile acids. The DKO mice displayed a very mild phenotype and, like the $Bsep^{-/-}$ mice, produced more β-MCA and THBA, while reducing the amount of CA secreted into bile (Fig. 3C and supplemental Table S2). This hydrophilic shift of bile acids seen in the $Bsep^{-/-}$ and DKO mice appears to be absent in the $Mdr2^{-/-}$ mice. The molecular trigger for this hydrophilic shift is not known and may be complex; however, we speculate that an accumulation of hydrophobic bile acid to some critical intrahepatic concentration may be required. The $Mdr2^{-/-}$ mice may not be able achieve such a concentration, because they carry a functional Bsep transporter protein, thereby maintaining a relatively lower level of intrahepatic hydrophobic bile acid. It is noteworthy that the total bile acid in the livers of $Bsep^{-/-}$ and DKO mice is severalfold higher than in the $Mdr2^{-/-}$ mice, consistent with the concept that a rise in hydrophobic bile acids could trigger P450 hydroxylases to reduce the intrahepatic concentration of hydrophobic bile acids, while the hydrophilic bile acids accumulate, resulting in the dramatic shift to a more hydrophilic bile acid composition in $Bsep^{-/-}$ and DKO mice. This hepatoprotective response appears to coincide with a change in expression of the *Cyp2c* family genes, downstream of Cyp27a1 in the production of MCA (31), particularly *Cyp2c55. Cyp2c70* and nine other members of the *Cyp2c* family, plus the bile acid 6β-hydroxylase *Cyp3a11* (32, 45), were expressed at higher levels in the $Bsep^{-/-}$ and/or DKO livers than in the $Mdr2^{-/-}$ mouse, making these likely candidates for the enzymes responsible for THBA production from trihydroxyl bile acids in $Bsep^{-/-}$ and DKO mice. Taken together, the dramatic hydrophilic shift of bile acid composition, coupled with the presence of an alternative canalicular transporter with the ability to transport hydrophilic bile acids, to promote bile flow in the DKO mice, protect them from the toxicity of nonmicelle-bound bile acids in the bile duct.

Bile acids can be genotoxins and cause DNA damage (46–51). Thus, it is not surprising that, when the toxicity of the primary bile acids is unleashed in the absence of complexing lipids, we observe over 6,000 gene-expression changes in the liver of $Mdr2^{-/-}$ mice, compared with their DKO littermates and WT mice. This is consistent with the work of Katzenellenbogen et al. (44), who also showed that at least 15 functional categories of genes were affected in the $Mdr2^{-/-}$ mice. It is therefore remarkable that, in the present study, the $Bsep^{-/-}$ mutation was able to epistatically suppress more than 4,000 of the $Mdr2^{-/-}$-associated gene-expression changes. The DKO mice do not develop any of the progressive PSC-like features of the $Mdr2^{-/-}$ mice, even after 13.5 months, even though the hydrophilic bile acids in these mice were still not complexed with lipids. We believe that this is the clearest demonstration to date of the hepatoprotective nature of hydrophilic bile acids. It is noteworthy that reducing the hydrophobicity of the bile acids appears to be a common adaptive reaction to cholestatic stress in patients (52, 53).

To determine whether THBA played a direct functional role in alleviating liver damage, we showed that synthetic THBAs, when administered intravenously to mice, are taken up from the bloodstream into the liver, conjugated, and secreted into the bile canaliculus (by BSEP), where they act as osmotic drivers of bile flow, as other bile acids are (Fig. 5A). We also showed that feeding $Mdr2^{-/-}$ mice with a 1% synthetic THBA diet resulted in significantly reduced relative liver weight, a more favorable liver indicator profile in plasma, and reduced gallstone formation (Fig. 5B). These results are consistent with THBA playing a direct role in alleviating liver damage caused by the $Mdr2^{-/-}$ mutation. However, the feeding of THBA did not restore the $Mdr2^{-/-}$ mice to the full DKO phenotype; notably lacking was any significant improvement in liver fibrosis. We note that the feeding regime used did not achieve the concentration of THBA and degree of bile acid hydrophilicity, found in the liver and bile of the DKO mice (compare Fig. 6A, B with Fig. 3A, B). Although supplementation with synthetic THBA dramatically reduced CA in the bile of the $Mdr2^{-/-}$ mice (Fig. 6B), their bile acid profile was still less hydrophilic, with much less THBA, than was seen in the DKO mice. It appears that the vast majority of the THBA fed to the $Mdr2^{-/-}$ mice passed through into the feces and was not efficiently absorbed (Fig. 6B). It is possible that better hepatoprotection by THBA might be achieved were a THBA with better oral bioavailability used instead, because the biology of the DKO clearly shows that adequate biliary secretion of sufficiently hydrophilic bile acids can fully protect these mice from the toxicity due to the lack of PC in their bile. Therefore, the potential for THBAs to act as therapeutics for PSC, and other liver pathologies brought on by abnormalities of bile flow (cholestases), will be of considerable interest for future studies.

In conclusion, the present study shows that in cholestasis, the concentration of toxic bile acids is the determining factor that leads to progressive liver injury. Hydrophilic bile acids, such as THBAs, in concert with an enabled canalicular transporter, were hepatoprotective, even on the $Mdr2^{-/-}$ genetic background, where hydrophilic bile acids,

whether produced endogenously or introduced orally, encounter a biliary tract entirely without the cytoprotection of PC in the bile.

REFERENCES

1. Wang, R., J. A. Sheps, and V. Ling. 2011. ABC transporters, bile acids, and inflammatory stress in liver cancer. *Curr. Pharm. Biotechnol.* **12:** 636–646.

2. Chiang, J. Y. 2017. Recent advances in understanding bile acid homeostasis. *F1000Res.* **6:** 2029.

3. Jansen, P. L., A. Ghallab, N. Vartak, R. Reif, F. G. Schaap, J. Hampe, and J. G. Hengstler. 2017. The ascending pathophysiology of cholestatic liver disease. *Hepatology.* **65:** 722–738.

4. Cai, S. Y., and J. L. Boyer. 2017. The role of inflammation in the mechanisms of bile acid-induced liver damage. *Dig. Dis.* **35:** 232–234.

5. Morotti, R. A., F. J. Suchy, and M. S. Magid. 2011. Progressive familial intrahepatic cholestasis (PFIC) type 1, 2, and 3: a review of the liver pathology findings. *Semin. Liver Dis.* **31:** 3–10.

6. Jacquemin, E. 2012. Progressive familial intrahepatic cholestasis. *Clin. Res. Hepatol. Gastroenterol.* **36(Suppl 1):** S26–S35.

7. Childs, S., R. L. Yeh, E. Georges, and V. Ling. 1995. Identification of a sister gene to P-glycoprotein. *Cancer Res.* **55:** 2029–2034.

8. Gerloff, T., B. Stieger, B. Hagenbuch, J. Madon, L. Landmann, J. Roth, A. F. Hofmann, and P. J. Meier. 1998. The sister of P-glycoprotein represents the canalicular bile salt export pump of mammalian liver. *J. Biol. Chem.* **273:** 10046–10050.

9. Wang, R., M. Salem, I. M. Yousef, B. Tuchweber, P. Lam, S. J. Childs, C. D. Helgason, C. Ackerley, M. J. Phillips, and V. Ling. 2001. Targeted inactivation of sister of P-glycoprotein gene (spgp) in mice results in nonprogressive but persistent intrahepatic cholestasis. *Proc. Natl. Acad. Sci. USA.* **98:** 2011–2016.

10. Jansen, P. L., S. S. Strautnieks, E. Jacquemin, M. Hadchouel, E. M. Sokal, G. J. Hooiveld, J. H. Koning, A. De Jager-Krikken, F. Kuipers, F. Stellaard, et al. 1999. Hepatocanalicular bile salt export pump deficiency in patients with progressive familial intrahepatic cholestasis. *Gastroenterology.* **117:** 1370–1379.

11. Knisely, A. S. 2000. Progressive familial intrahepatic cholestasis: a personal perspective. *Pediatr. Dev. Pathol.* **3:** 113–125.

12. Strautnieks, S. S., J. A. Byrne, L. Pawlikowska, D. Cebecauerova, A. Rayner, L. Dutton, Y. Meier, A. Antoniou, B. Stieger, H. Arnell, et al. 2008. Severe bile salt export pump deficiency: 82 different ABCB11 mutations in 109 families. *Gastroenterology.* **134:** 1203–1214.

13. Scheimann, A. O., S. S. Strautnieks, A. S. Knisely, J. A. Byrne, R. J. Thompson, and M. J. Finegold. 2007. Mutations in bile salt export pump (ABCB11) in two children with progressive familial intrahepatic cholestasis and cholangiocarcinoma. *J. Pediatr.* **150:** 556–559.

14. Lam, P., R. Wang, and V. Ling. 2005. Bile acid transport in sister of P-glycoprotein (ABCB11) knockout mice. *Biochemistry.* **44:** 12598–12605.

15. Wang, R., P. Lam, L. Liu, D. Forrest, I. M. Yousef, D. Mignault, M. J. Phillips, and V. Ling. 2003. Severe cholestasis induced by cholic acid feeding in knockout mice of sister of P-glycoprotein. *Hepatology.* **38:** 1489–1499.

16. Smit, J. J., A. H. Schinkel, R. P. Oude Elferink, A. K. Groen, E. Wagenaar, L. van Deemter, C. A. Mol, R. Ottenhoff, N. M. van der Lugt, M. A. van Roon, et al. 1993. Homozygous disruption of the murine mdr2 P-glycoprotein gene leads to a complete absence of phospholipid from bile and to liver disease. *Cell.* **75:** 451–462.

17. Lucena, J. F., J. I. Herrero, J. Quiroga, B. Sangro, J. Garcia-Foncillas, N. Zabalegui, J. Sola, M. Herraiz, J. F. Medina, and J. Prieto. 2003. A multidrug resistance 3 gene mutation causing cholelithiasis, cholestasis of pregnancy, and adulthood biliary cirrhosis. *Gastroenterology.* **124:** 1037–1042.

18. Mauad, T. H., C. M. van Nieuwkerk, K. P. Dingemans, J. J. Smit, A. H. Schinkel, R. G. Notenboom, M. A. van den Bergh Weerman, R. P. Verkruisen, A. K. Groen, R. P. Oude Elferink, et al. 1994. Mice with homozygous disruption of the mdr2 P-glycoprotein gene. A novel animal model for studies of nonsuppurative inflammatory cholangitis and hepatocarcinogenesis. *Am. J. Pathol.* **145:** 1237–1245.

19. Ikenaga, N., S. B. Liu, D. Y. Sverdlov, S. Yoshida, I. Nasser, Q. Ke, P. M. Kang, and Y. Popov. 2015. A new Mdr2(−/−) mouse model of sclerosing cholangitis with rapid fibrosis progression, early-onset portal hypertension, and liver cancer. *Am. J. Pathol.* **185:** 325–334.

20. Fickert, P., A. Fuchsbichler, M. Wagner, G. Zollner, A. Kaser, H. Tilg, R. Krause, F. Lammert, C. Langner, K. Zatloukal, et al. 2004. Regurgitation of bile acids from leaky bile ducts causes sclerosing cholangitis in Mdr2 (Abcb4) knockout mice. *Gastroenterology.* **127:** 261–274.

21. Van Nieuwkerk, C. M., R. P. Elferink, A. K. Groen, R. Ottenhoff, G. N. Tytgat, K. P. Dingemans, M. A. Van Den Bergh Weerman, and G. J. Offerhaus. 1996. Effects of ursodeoxycholate and cholate feeding on liver disease in FVB mice with a disrupted mdr2 P-glycoprotein gene. *Gastroenterology.* **111:** 165–171.

22. van Nieuwerk, C. M., A. K. Groen, R. Ottenhoff, M. van Wijland, M. A. van den Bergh Weerman, G. N. Tytgat, J. J. Offerhaus, and R. P. Oude Elferink. 1997. The role of bile salt composition in liver pathology of mdr2 (−/−) mice: differences between males and females. *J. Hepatol.* **26:** 138–145.

23. Wang, R., L. Liu, J. A. Sheps, D. N. Forrest, A. F. Hofmann, L. R. Hagey, and V. Ling. 2013. Defective canalicular transport and toxicity of dietary ursodeoxycholic acid in the abcb11−/− mouse: transport and gene expression studies. *Am. J. Physiol. Gastrointest. Liver Physiol.* **305:** G286–G294.

24. Iida, T., I. Komatsubara, S. Yoda, J. Goto, T. Nambara, and F. C. Chang. 1990. Potential bile acid metabolites. 16. Synthesis of stereoisomeric 3 alpha,6,7,12 alpha-tetrahydroxy-5 beta-cholanoic acids. *Steroids.* **55:** 530–539.

25. Aggarwal, S. K., A. K. Batta, G. Salen, and S. Shefer. 1992. Synthesis of 3 alpha,6 beta,7 alpha,12 beta- and 3 alpha,6 beta,7 beta,12 beta-tetrahydroxy-5 beta-cholanoic acids. *Steroids.* **57:** 107–111.

26. Han, J., Y. Liu, R. Wang, J. Yang, V. Ling, and C. H. Borchers. 2015. Metabolic profiling of bile acids in human and mouse blood by LC-MS/MS in combination with phospholipid-depletion solid-phase extraction. *Anal. Chem.* **87:** 1127–1136.

27. Qiu, Y. L., J. Y. Gong, J. Y. Feng, R. X. Wang, J. Han, T. Liu, Y. Lu, L. T. Li, M. H. Zhang, J. A. Sheps, et al. 2017. Defects in myosin VB are associated with a spectrum of previously undiagnosed low gamma-glutamyltransferase cholestasis. *Hepatology.* **65:** 1655–1669.

28. Mortazavi, A., B. A. Williams, L. McCue, L. Schaeffer, and B. Wold. 2008. Mapping and quantifying mammalian transcriptomes by RNA-Seq. *Nat. Methods.* **5:** 621–628.

29. Benjamini, Y., and Y. Hochberg. 1995. Controlling the false discovery rate: a practical and powerful approach to multiple testing. *J. R. Stat. Soc. B.* **57:** 289–300.

30. Anders, S., and W. Huber. 2010. Differential expression analysis for sequence count data. *Genome Biol.* **11:** R106.

31. Takahashi, S., T. Fukami, Y. Masuo, C. N. Brocker, C. Xie, K. W. Krausz, C. R. Wolf, C. J. Henderson, and F. J. Gonzalez. 2016. Cyp2c70 is responsible for the species difference in bile acid metabolism between mice and humans. *J. Lipid Res.* **57:** 2130–2137.

32. Wahlström, A., S. Al-Dury, M. Ståhlman, F. Bäckhed, and H. U. Marschall. 2017. Cyp3a11 is not essential for the formation of murine bile acids. *Biochem. Biophys. Rep.* **10:** 70–75.

33. Hirohashi, T., H. Suzuki, H. Takikawa, and Y. Sugiyama. 2000. ATP-dependent transport of bile salts by rat multidrug resistance-associated protein 3 (Mrp3). *J. Biol. Chem.* **275:** 2905–2910.

34. Schuetz, E. G., S. Strom, K. Yasuda, V. Lecureur, M. Assem, C. Brimer, J. Lamba, R. B. Kim, V. Ramachandran, B. J. Komoroski, et al. 2001. Disrupted bile acid homeostasis reveals an unexpected interaction among nuclear hormone receptors, transporters, and cytochrome P450. *J. Biol. Chem.* **276:** 39411–39418.

35. Zelcer, N., G. Reid, P. Wielinga, A. Kuil, I. Van Der Heijden, J. D. Schuetz, and P. Borst. 2003. Steroid and bile acid conjugates are substrates of human multidrug-resistance protein (MRP) 4 (ATP-binding cassette C4). *Biochem. J.* **371:** 361–367.

36. Alnouti, Y. 2009. Bile Acid sulfation: a pathway of bile acid elimination and detoxification. *Toxicol. Sci.* **108:** 225–246.

37. Fang, Z. Z., R. R. He, Y. F. Cao, N. Tanaka, C. Jiang, K. W. Krausz, Y. Qi, P. P. Dong, C. Z. Ai, X. Y. Sun, et al. 2013. A model of in vitro UDP-glucuronosyltransferase inhibition by bile acids predicts possible metabolic disorders. *J. Lipid Res.* **54:** 3334–3344.

38. Singh, S. V., T. Leal, and Y. C. Awasthi. 1988. Inhibition of human glutathione S-transferases by bile acids. *Toxicol. Appl. Pharmacol.* **95:** 248–254.

39. Hofmann, A. F. 2004. Detoxification of lithocholic acid, a toxic bile acid: relevance to drug hepatotoxicity. *Drug Metab. Rev.* **36:** 703–722.

40. Megaraj, V., T. Iida, P. Jungsuwadee, A. F. Hofmann, and M. Vore. 2010. Hepatobiliary disposition of 3alpha,6alpha,7alpha,12alpha-tetrahydroxy-cholanoyl taurine: a substrate for multiple canalicular transporters. *Drug Metab. Dispos.* **38:** 1723–1730.

41. Chiang, J. Y. 2009. Bile acids: regulation of synthesis. *J. Lipid Res.* **50:** 1955–1966.

42. Bodewes, F. A., M. J. Bijvelds, W. de Vries, J. F. Baller, A. S. Gouw, H. R. de Jonge, and H. J. Verkade. 2015. Cholic acid induces a Cftr dependent biliary secretion and liver growth response in mice. *PLoS One.* **10:** e0117599.

43. Wang, R., H-L. Chen, L. Liu, J. A. Sheps, M. J. Phillips, and V. Ling. 2009. Compensatory role of P-glycoproteins in knockout mice lacking the bile salt export pump. *Hepatology.* **50:** 948–956.

44. Katzenellenbogen, M., O. Pappo, H. Barash, N. Klopstock, L. Mizrahi, D. Olam, J. Jacob-Hirsch, N. Amariglio, G. Rechavi, L. A. Mitchell, et al. 2006. Multiple adaptive mechanisms to chronic liver disease revealed at early stages of liver carcinogenesis in the Mdr2-knockout mice. *Cancer Res.* **66:** 4001–4010.

45. Hrycay, E., D. Forrest, L. Liu, R. Wang, J. Tai, A. Deo, V. Ling, and S. Bandiera. 2014. Hepatic bile acid metabolism and expression of cytochrome P450 and related enzymes are altered in Bsep (−/−) mice. *Mol. Cell. Biochem.* **389:** 119–132.

46. Totsuka, Y., R. Nishigaki, S. Enomoto, T. Takamura-Enya, K. Masumura, T. Nohmi, N. Kawahara, T. Sugimura, and K. Wakabayashi. 2005. Structures and biological properties of DNA adducts derived from N-nitroso bile acid conjugates. *Chem. Res. Toxicol.* **18:** 1553–1562.

47. Jenkins, G. J., F. R. D'Souza, S. H. Suzen, Z. S. Eltahir, S. A. James, J. M. Parry, P. A. Griffiths, and J. N. Baxter. 2007. Deoxycholic acid at neutral and acid pH, is genotoxic to oesophageal cells through the induction of ROS: The potential role of anti-oxidants in Barrett's oesophagus. *Carcinogenesis.* **28:** 136–142.

48. Payne, C. M., C. Bernstein, K. Dvorak, and H. Bernstein. 2008. Hydrophobic bile acids, genomic instability, Darwinian selection, and colon carcinogenesis. *Clin. Exp. Gastroenterol.* **1:** 19–47.

49. Senthong, P., C. L. Millington, O. J. Wilkinson, A. S. Marriott, A. J. Watson, O. Reamtong, C. E. Eyers, D. M. Williams, G. P. Margison, and A. C. Povey. 2013. The nitrosated bile acid DNA lesion O6-carboxymethylguanine is a substrate for the human DNA repair protein O6-methylguanine-DNA methyltransferase. *Nucleic Acids Res.* **41:** 3047–3055.

50. Terasaki, M., Y. Totsuka, K. Nishimura, K. Mukaisho, K. H. Chen, T. Hattori, T. Takamura-Enya, T. Sugimura, and K. Wakabayashi. 2008. Detection of endogenous DNA adducts, O-carboxymethyl-2′-deoxyguanosine and 3-ethanesulfonic acid-2′-deoxycytidine, in the rat stomach after duodenal reflux. *Cancer Sci.* **99:** 1741–1746.

51. Ueyama, Y., Y. Monden, X. B. He, C. X. Lin, M. A. Momen, S. Mimura, and A. Umemoto. 2002. Effects of bile acids on 2-amino-1-methyl-6-phenylimidazo[4,5-b]pyridine-induced aberrant crypt foci and DNA adduct formation in the rat colon. *J. Exp. Clin. Cancer Res.* **21:** 577–583.

52. Liu, T., R. X. Wang, J. Han, C. Z. Hao, Y. L. Qiu, Y. Y. Yan, L. T. Li, N. L. Wang, J. Y. Gong, Y. Lu, et al. 2018. Comprehensive bile acid profiling in hereditary intrahepatic cholestasis: Genetic and clinical correlations. *Liver Int.* **38:** 1676–1685.

53. Lee, C. S., A. Kimura, J. F. Wu, Y. H. Ni, H. Y. Hsu, M. H. Chang, H. Nittono, and H. L. Chen. 2017. Prognostic roles of tetrahydroxy bile acids in infantile intrahepatic cholestasis. *J. Lipid Res.* **58:** 607–614.

54. Babicki, S., D. Arndt, A. Marcu, Y. Liang, J. R. Grant, A. Maciejewski, and D. S. Wishart. 2016. Heatmapper: web-enabled heat mapping for all. *Nucleic Acids Res.* **44:** W147–W153.